Niche exclusion of a lung pathogen in mice with designed probiotic communities

Kelsey E Hern[1], Ashlee M Phillips[2], Catherine M. Mageeney[3], Kelly P. Williams[4], Anupama Sinha[3], Hans K Carlson[5], Nicole M Collette[2], Steven S Branda[3], Adam P Arkin[5,6]

1. Department of Plant and Microbial Biology, University of California Berkeley, Berkeley, CA, United States
2. Division of Biosciences and Biotechnology, Lawrence Livermore National Laboratory, Livermore, CA, United States
3. Department of Biotechnology and Bioengineering, Sandia National Laboratories, Livermore, CA, United States
4. Department of Systems Biology, Sandia National Laboratories, Livermore, CA, United States
5. Division of Environmental Genomics and Systems Biology, Lawrence Berkeley National Laboratory, Berkeley, CA, United States
6. Department of Biological Engineering, University of California Berkeley, Berkeley, CA, United States

Abstract

For years, the airway microbiota have been theorized to be gatekeepers of respiratory health, as pathogens entering the airway make contact with resident microbes prior to or coincident with their interaction with host cells. Thus, modification of the native airway community may serve as a means of altering the local environment in favor of health. While probiotic supplementation to prevent pathogen infiltration has been explored extensively in the gut, little has been done to study this phenomenon in the lower respiratory tract. In this work, we hypothesize that synthetic bacterial communities introduced into the airway can serve as prophylactic countermeasures against infection by a model bacterial pathogen (*Burkholderia thailandensis*) in mice. We demonstrate that understanding of antagonistic interactions between a pathogen and airway microbiota *in vitro* can guide identification of probiotics with protective capabilities *in vivo*. While production of secondary metabolites appears to play a role in pathogen antagonism, exploitative competition appears to be the predominant mechanism by which the organisms studied here inhibit *B. thailandensis*. Specifically we show that niche overlap and resource competition between the probiotic and pathogen are predictive of probiotic performance *in vivo*. This work serves as a foundation for the rational design of probiotic communities for protection against and treatment of respiratory infections.

Introduction

Every mammalian body compartment that opens to the outside world has microbial life associated with it[1]. Until recently, the healthy lung was thought to be a sterile environment; however, recent work has demonstrated that the lower respiratory tract is colonized by a complex and roughly stable microbiome that impacts the health of the host[2–4]. For years, the airway microbiota have been theorized to be gatekeepers of respiratory health, as pathogens entering the airway make contact with its microbiota prior to or coincident with their interactions with host cells[3]. While the latter interactions have been studied in detail, little is known about pathogen-microbiome interactions in the airway.

It has been hypothesized that pathogen establishment in the airway could be halted by its microbiota through either indirect or direct competition with the pathogen[3,5,6]. During indirect competition, airway microbiota would modulate the host immune response to increase surveillance, promoting rapid recognition and clearance of foreign microbes including pathogenic organisms. During direct competition, the airway microbiota would competitively exclude a pathogen through production of inhibitory specialized metabolites, and/or by occupying a nutritional niche that would otherwise be used by the pathogen. Enhancement of these defense mechanisms might be achieved through addition of health-promoting microbes (probiotics) directly to the lower airway, an approach that has been demonstrated to prevent pneumococcal and *Pseudomonas aeruginosa* infection previously[7,8].

While these studies have shed light on the utility of lower airway probiotics for preventing two specific infections, greater understanding of the principles that dictate probiotic efficacy would allow rapid identification of probiotics with therapeutic potential against many pathogenic targets. To enable development of these therapies in the future, pipelines for probiotic nomination need to be made which can rapidly and cheaply identify effective therapies. Further, systematic analysis of the mechanism of action of these probiotics would allow fine-tuned control of their activity allowing for more reliable therapeutic outcomes in the clinic.

Here, we seek to fill this gap in knowledge by systematically characterizing factors that make efficacious lower airway probiotics that can competitively exclude a model pathogen, *Burkholderia thailandensis* (*Bt*), from the lung environment. Specifically, we hypothesize that negative microbial interactions between a probiotic and pathogen better protect the host against infection. Our systematic study of the microbial ecology of these organisms enables development of a pipeline for nomination of effective single and multi-organism probiotics that, to this point, remain underdeveloped. We show that

using our pipeline, we can accurately identify pairwise combinations of organisms with synergistic activity against *Bt*. Finally, we test the ability of these prophylactically administered probiotics to promote survival during a challenge with *Bt in vivo*.

Results

Isolation and Characterization of Candidate Probiotics

To develop a system for testing the efficacy of lower airway probiotics in preventing infection, it was first necessary to identify a suitable pathogen to investigate. *Burkholderia thailandensis* (*Bt*) is a pathogen of mice that is genomically similar to several human pathogens including *Burkholderia pseudomallei, Burkholderia mallei* and organisms of the *Burkholderia cepacia complex,* the latter of which poses a high risk of mortality for cystic fibrosis patients[9–13]. Thus, *Burkholderia thailandensis* is an appropriate subject of study for our purposes as it is safe, infectious in mice and a good model of several pathogens with clinical relevance.

To acquire candidate probiotics for use in the lower airway, we sought organisms which would be able to survive in the lower airway for an extended period of time and be capable of tolerating its low-nutrient environment[14]. We hypothesized that organisms directly isolated from the airway would fulfill this criterion, as they are already well-adapted to the environment and may be more immunologically tolerated by the host. To isolate candidate probiotics, the trachea and lungs were collected from C57Bl/6j mice, homogenized, and plated onto five different solid growth media, either directly or after an initial period of culture in blood bottles. Bacterial colonies were repeatedly streaked on LB agar to recover clonal isolates for whole-genome sequencing. Twenty eight of these isolates were further characterized for use as lower airway probiotics.

Prior work on the lung microbiome has led to the widely held hypothesis that many of its constituents originate from the oral and/or nasal microbiome and are unable to actively replicate and persist in the lower airway[15,16]. We therefore sought to identify airway isolates that are capable of active growth in the lower respiratory tract, with the supposition that they should be better equipped to re-colonize the airway and compete against an invading pathogen. To do this, the airway isolates were cultured in lung simulating medium (LSM), which is based on the nutrient composition of sputum samples from cystic fibrosis patients, and therefore is thought to approximate the nutritional environment of the lower respiratory tract[17]. We found that 10 of 28 airway isolates tested were capable of robust growth (>1 doubling within 48 hours) in LSM

(Figure S1). These 10 isolates, and model pathogen *Bt*, are arrayed on a phylogenomic tree (Figure 1A), and are henceforth referred to as candidate probiotics (CPs).

Next, we aimed to identify CPs capable of competing against *Bt* during co-culture in LSM, with the hypothesis that they might also compete against *Bt* in the lower respiratory tract and therefore serve as efficacious probiotics. Expression of competitive phenotypes is dependent on several factors including the cell density relative to the available resources[18,19]. Accordingly, we decided to assay competition in LSM across varying cell densities, with the hypothesis that this would enable us to capture information about CP potency. Each CP was co-cultured with *Bt* in LSM at different relative ratios (Figure 1B). We found that the CPs showed a range of activities, including negative interactions (Figure 1C top 6 plots) and positive interactions (Figure 1C lower 4 plots) with *Bt*; the potency of each CP, as indicated by IC50 value, is shown in Table 1.

Investigation of interference competition

Next, we sought to better understand the mechanism(s) of the observed negative interactions. We hypothesized that negative interactions could be direct, through chemical attack (interference competition); or indirect, through resource consumption (exploitative competition). First, we investigated the presence of interference competition by growing *Bt* in sterilized co-culture supernatant from itself and a CP. We predicted that if *Bt*-inhibiting secondary metabolites were produced by a given CP during co-culture in LSM, then the conditioned medium recovered from the co-culture would display inhibitory activity against *Bt*. To test this, each negatively-interacting CP was co-cultured with *Bt*, filter sterilized and combined with double-concentrated LSM to serve as medium for *Bt* growth curves (Figure 2A). We found that the co-culture supernatant from one airway isolate (CP8) significantly reduced growth of *Bt* compared to supernatant from a *Bt* monoculture (negative control) (Figure 2B). This indicated that CP8 likely produced a specialized metabolite and was engaging in interference competition.

To understand the degree to which CP8's secondary metabolite is responsible for mediating the competitive phenotype observed in Figure 1C, we aimed to create a knockout of this molecule in CP8. From prior analyses, CP8 is predicted to encode production of 22 specialized metabolites[20]. The synthesis of all of the top hits are dependent on *sfp*, a phosphopantetheinyl transferase which catalyzes conversion of these metabolites into their active holo-form. Therefore, we hypothesized that knocking out *sfp* from CP8 would result in an isolate with an inability to produce a specialized metabolite with inhibitory capabilities against *Bt*. A clean deletion of the *sfp* gene was made in CP8 and an agar diffusion assay was performed which showed a reduction in

the zone of inhibition indicating that interference competition was reduced (Figure 2C). Finally, a competition assay was performed using the CP8Δ*sfp* mutant. The mutant showed reduced inhibitory activity compared to wildtype CP8 and, in contrast, demonstrated a positive interaction with *Bt* when interference competition was disrupted (Figure 2D).

Investigation of niche overlap as a predictor of competition

While interference competition appeared to be the primary mode of inhibition for CP8, 5 other CPs showed a negative interaction with *Bt* but did not appear to produce specialized metabolites. We hypothesized that inhibition with these 5 isolates was due to exploitative competition whereby the passive consumption of a limiting resource by the CP would reduce the supply to *Bt*.

The Redfield Ratio describes the stoichiometric relationship between carbon, nitrogen and phosphorous which supports life on earth and is canonically 106:16:1. Recent work has shown that this ratio is variable across body sites with areas like the mouth and gut being more carbon rich and the upper airways being relatively carbon poor[21]. Similar to the upper airway, LSM is carbon limiting with a C:N:P ratio of approximately 88:14:1. This indicates that carbon may be the limiting nutrient and thus would be competed for by the CPs and *Bt*. Thus, we predicted that if carbon was limiting, adding carbon to LSM would reduce competition. To test this, LSM was supplemented with 43mM glucose to increase the C:N:P ratio to 101:14:1. In Figure 3A, we observed a leftward shift of the dose-response curve for CP7 in the additional carbon condition and a significant reduction in inhibition at a 1:100 ratio (Figure 3B). A similar result is observed when the same experiment is conducted in CP19 (Figure S2). This result suggests that there is a reduction in competition with increased carbon abundance and indicates that, under the carbon limiting conditions of the lung, carbon is the primary nutrient for which CPs and *Bt* are competing.

Further, we sought to explore the extent to which competition for carbon with *Bt* could predict inhibitory capabilities of each CP. To do this, we assayed the growth of each CP and *Bt* in each individual carbon source from LSM to determine which carbon sources could be utilized by each organism (Figure 3C). *Bt* shows a wide range of metabolic potential and is able to grow on every carbon source presented except for ornithine. This is perhaps unsurprising as it has been shown previously that pathogens acquire new metabolisms in order to survive in their host[22]. Conversely, the CPs display diverse metabolic activity with CP4 and CP7 appearing most similar (Figure 3C).

Each carbon source in LSM is used both for production of biomass as well as the primary electron donor to generate energy via aerobic respiration. In the niche exclusion hypothesis, a competitive advantage can be obtained for an organism that is able to consume those resources that would otherwise fuel aerobic respiration of a competitor. We therefore hypothesized that those CPs that were capable of competing for more carbon-derived electrons with *Bt* would have more potent inhibition against the pathogen (Figure 3D). On this assumption, we built a simple index of niche overlap which weights each carbon source in LSM utilized by a given CP by the theoretical electron contribution of that given source with the belief that such a metric could identify probiotics capable of achieving maximal niche coverage. Niche Index (NI) is calculated as follows:

Electron equivalents for each mole of carbon source are calculated based on concentration and oxidation-reduction half-reaction are held in vector $\vec{E}$.

$$\vec{E} = \begin{pmatrix} glucose \\ lactate \\ asparticacid \\ threonine \\ serine \\ glutamine \\ proline \\ glycine \\ alanine \\ cysteine \\ valine \\ methionine \\ isoleucine \\ leucine \\ tyrosine \\ phenylalanine \\ ornthine \\ lysine \\ histidine \\ tryptophan \\ arginine \end{pmatrix},$$

The weighted value for each carbon source is:

$$\overrightarrow{W} = \frac{\overrightarrow{E}}{E_{glucose}} \tag{1}$$

For all CPs and *Bt*, a carbon utilization vector is generated. If a carbon source is consumed, then i = 1, if it is not able to be consumed, then i = 0.

$$\overrightarrow{CU_{CP}} = \begin{bmatrix} i_1 \\ i_2 \\ i_3 \\ i_4 \\ \vdots \\ i_n \end{bmatrix},$$

To calculate the Niche Index of each CP with *Bt*, the equation is:

$$NI_{CP} = \frac{[\vec{CU}_{CP} \odot \vec{CU}_{Bt}] \cdot \vec{W}}{[\vec{CU}_{Bt} \cdot \vec{W}] - [CU_{CP,orn} \cdot W]} \tag{2}$$

NI is higher when a given CP shares a greater number of electrons with *Bt* and appears to be a good predictor of inhibitory activity against *Bt* at a 1:1 ratio (Table 1 and Figure 3E). Notably, CP8 is excluded from this analysis as its potency is expected to be primarily a result of secondary metabolite production rather than carbon consumption. Additionally, robust regression analysis showed CP26 as an outlier and thus it is not included in the analysis (Figure S3). While here we have used Niche Index to calculate niche overlap between CPs and *Bt* in LSM, this model is generalizable and can be used to calculate the niche overlap between organisms in any media with a known molar carbon composition.

To confirm our hypothesis that those organisms that compete for more carbon-derived electrons with *Bt* are better competitors, we performed exometabolomics on supernatant from 3 CPs. These 3 CPs represent a range of inhibition strengths and niche indexes, with CP7 being the most potent (IC50 = 0.001172 NI = 0.875), CP19 displaying moderate potency (IC50 = 0.006604 NI = 0.775) and CP8 being the least potent (IC50 = 2.316 NI = 0.351). Each of these CPs was combined with *Bt* at their respective IC90 and co-incubated for 36 hours. Supernatant from these CPs at 36 hours show that more potent CPs consume a statistically greater amount of carbon from the media than less potent CPs (Figure 3F). At 24 hours where the degree of inhibition of *Bt* by each CP is the same, more potent competitors achieve *Bt* suppression by consuming fewer carbon-derived electrons than less potent competitors (Figure 3G). This led us to

hypothesize that certain carbon sources were being prioritized allowing better competitors to have the same net effect on *Bt* while consuming fewer electrons. Further, we speculated that if high priority carbon sources were to be identified, perhaps the consumption of a smaller set of these high priority carbon sources could predict activity with similar accuracy to the Niche Index.

From the exometabolomics data, consumption of three carbon sources, lactate, proline and aspartic acid are prioritized more at 24 hours by the most potent candidate probiotic, CP7, than the least potent, CP8 (Figure 3H). Furthermore, we found that a CPs ability to generate biomass on lactate was a good predictor of its ability to inhibit the pathogen suggesting that the ability to consume lactate in co-culture may be important for pathogen control (Figure 3I). Overall, these results demonstrate that different resources may have different competitive effects on an interaction. While these results are promising building blocks for the development of a metric of activity based upon a smaller feature set, a larger screen of candidate probiotics may be necessary to understand the utility of these features for good prediction.

Niche overlap predicts combination efficacy

While our work in Figure 1 showed that 6 of the CPs were potent inhibitors of *Bt* in individual co-culture, 4 were poor inhibitors or promoted growth of *Bt*. Having found that NI was a good predictor of individual CP potency *in vitro*, we hypothesized that this metric could be altered to identify pairwise combinations of poor-performing CPs with enhanced antagonism. To do this, we created a new metric, the Niche Index Fraction (NIF), which is composed of the niche overlap between two given CPs divided by the niche overlap between these two CPs and *Bt* (Figure 4A). It is calculated as follows:

First, the overlap between two CPs is generated and is weighted by the relative electron contribution of each carbon source

$$y = [\vec{CU}_{CPx} \odot \vec{CU}_{CPy}] \cdot \vec{W} \tag{3}$$

Total carbon-derived electron utilization is calculated for both CPs

$$p = \vec{X}_{CPx,CPy} \cdot \vec{W}, \textit{such that } p \textit{ is never } 0 \tag{4}$$

For which

$$\vec{X}_{CPx,CPy} = \begin{cases} CU_{i,CPx} = 1 = CU_{i,CPy}; 1 \\ CU_{i,CPx} = 0 = CU_{i,CPy}; 0 \\ CU_{i,CPx} \neq CU_{i,CPy}; 1 \end{cases} \tag{5}$$

Thus the niche overlap between two CPs is

$$NI_{CPx,CPy} = \frac{y}{p} \tag{6}$$

The niche overlap between two CPs and *Bt* is thus

$$NIF_{CPx,CPy} = \frac{NI_{CPx,CPy}}{[C\vec{U}_{Bt} \cdot \vec{W}] - [\vec{X}_{CPx,CPy,orn} \cdot \vec{W}]} \tag{7}$$

We calculated NIF for every pairwise combination of the 7 least antagonistic CPs from Figure 1. This generated a matrix of potential synergistic combinations (Figure 4B). We hypothesized that combinations with lower niche index fractions would indicate high niche overlap with *Bt* but low niche overlap between two isolates and were thus more likely to act synergistically to inhibit *Bt*. To test the ability of this metric to predict CP interactions, we chose to test pairwise combinations with the three lowest fractions as well as a combination with a moderate fraction and high fraction using competition assays.

In these assays, two CPs were combined at a 1:1 ratio such that the total CP concentration at a given ratio was the same as their individual CP counterparts. This enabled us to directly compare activity of an individual CP and the activity of a combination of two CPs at a given ratio as the total cell density was the same in each. From competition assays, we determined that NIF was able to predict synergistic combinations and non-synergistic combinations as reflected by their relative IC50 values (Figure 4C,D,E, Figure S4 and Table S1). Further, the combination with the largest leftward shift, CP19 and CP8 (Figure 4C) was determined to be synergistic via the Bliss independence model (Figure 4F). This model compares the observed

combination response to the predicted combination response of two drugs[23]. The drug combination is declared synergistic if the observed combination response is greater than the predicted combination response. Several other combinations with low niche index fractions showed similar results, however, Bliss independence index was only calculated in cases where both CPs individually demonstrate an inhibitory effect. Further study of NIF will be necessary to determine the generalizability of these phenomena.

For one combination, CP8 and CP19, we sought to understand the mechanism by which competition was being enhanced. First, to understand the effect of the interaction on all members of the co-culture, we performed growth curves of each individual strain in the CP8, CP19 and *Bt* when in co-culture (Figure S5). Reduced growth in co-culture of all three organisms classifies this antagonistic interaction as true competition. To better understand how CP8 and CP19 may enhance each other's antagonistic impact on *Bt*, we once again performed exometabolomics analysis on supernatant from this combination. At 24 hours, significantly more lactate was consumed per cell in the combination than by CP8/*Bt* co-culture or CP19/*Bt* co-culture ($p<0.0001$) (Figure 4G). Similarly to the single isolate studies, this result once again suggests that lactate utilization may be important for competition with *Bt* in an airway-simulating environment.

To further investigate how CP8 and CP19 act synergistically, we performed a competition assay using the CP8Δ*sfp* mutant in combination with CP19 to understand the degree to which secondary metabolite production was responsible for this synergistic effect (Figure 4H). When wildtype CP8 was replaced with the Δ*sfp* mutant, there was a significant reduction in *Bt* inhibitory activity compared to the wildtype CP8/CP19 combination. Together, these findings suggest that both carbon consumption and secondary metabolite production are important for activity of the CP8/CP19 combination and likely enable *Bt* inhibition activity (Figure 4I). While NIF suggests that coverage of the pathogen niche may be responsible for the observed synergies in other combinations, further investigation needs to be done to understand these interactions in more detail.

CPs provide protection against infection

Having observed the ability of the CPs to compete with *Bt* in an *in vitro* airway-simulating environment, we were encouraged to test their ability to confer protection against respiratory *Bt* infection *in vivo*. Firstly, we hypothesized that those CPs which colonized at high density over an extended period of time would provide better protection against *Bt* infection. To test the airway colonization capabilities of the CPs, we administered each to C57Bl/6j mice at 10^6 CFU via oropharyngeal aspiration (OPA). After a period of 7 days, the lungs and trachea were assessed for CP load via

CFU enumeration (Figure 5A). We found that several CPs were able to colonize the airway for the duration of the 7-day period (Figure 5B). We were particularly interested in those CPs displaying airway colonization (mean airway CFU load of >10 CFU), as these would seem most likely to be capable of protecting against respiratory *Bt* infection.

While we hypothesized from our *in vitro* work that direct competition between the CP and pathogen would confer the strongest protection against infection, immune modulation is also a potential mechanism by which probiotics confer protection. Therefore, we screened both colonizing and non-colonizing CPs for their ability to confer protection in a mouse model of respiratory *Bt* infection. In these studies, 10^6 CFU of each of 6 CPs was administered to the airway of C57Bl/6j mice via OPA. Following a period of 3, 5, or 7 days, *Bt* was administered to the airway and mortality was monitored for 10 days following *Bt* challenge (Figure 5C). Mice administered no CP prior to *Bt* challenge showed high mortality, only rarely surviving past day 4 (Figure 5D). In contrast, mice administered certain CPs prior to *Bt* challenge showed significantly reduced mortality (Figure 5E). Five of the six CPs were protective when administered 3 days prior to *Bt* challenge; CP17 was protective when administered at 3 or 5 days prior to *Bt* challenge; and CP19 was protective when administered at 3, 5, or 7 days prior to *Bt* challenge.

We observed that the most protective probiotics, CP19 and CP17, were predicted to have the highest niche overlap with *Bt* via their NI values and also showed an ability to inhibit in competition assays (Figure 1C). Furthermore, the CPs that did not inhibit *Bt* in competition assays yet do robustly colonize (Figure 5B) (i.e. CP13, CP20, and CP26) showed no significant protection when administered 5 or 7 days prior to *Bt* challenge (Figure 5E). A notable exception to this trend was CP8, which showed inhibition in competition assays as well as robust colonization, but showed no significant protection of mice challenged with *Bt*. This suggests that resource competition may be more predictive of the protective capabilities of a probiotic than secondary metabolite production. While it appears that the NI of a CP has some relationship to the efficacy and longevity of its protective effects, further investigation will need to be conducted to determine the extent to which niche overlap can be used to nominate efficacious probiotics in the future.

Discussion

The human respiratory tract microbiome composition has been linked to both respiratory health and the occurrence of respiratory infections[24]. As a result of this connection, manipulation of the lower airway microbiome is an attractive strategy for anti-infective

therapies. Airway microbiome modulation via supplementation with probiotics has previously shown success in preventing infections, however, these studies lack a more broad and systematic analysis which is necessary to learn generalizable principles for the design of efficacious lower airway probiotics[7,8].

In this work, we developed a system that probes interactions between airway-derived candidate probiotics (CPs) and a model respiratory pathogen *Burkholderia thailandensis*. From this exploration, we find that resource competition is the most frequent antagonistic phenotype in interactions between CPs and *Bt in vitro*. Specifically, competition for carbon seems to play an important role in these interactions. As a result a metric of niche overlap, Niche Index (NI), is indicative of CP inhibitory activity *in vitro*. Furthermore, we use these same principles to design combinations of CPs with enhanced antagonism against *Bt*. We explore the mechanism by which one combination, CP19 and CP8, exploits both resource competition and inhibitory metabolite production to its advantage in competing with *Bt*. Finally, we find that several CPs are able to re-colonize the mouse airway for at least 7 days and that two CPs (CP19 and CP17) significantly reduce mortality in mice subjected to otherwise lethal respiratory *Bt* challenge. While it appears that NI is indicative of the protective capabilities of a CP, further experiments will need to be done to determine if it can be used to formulate probiotics with clinical applicability.

The method described here is a step towards a more rapid, inexpensive and effective means of identifying efficacious probiotics, all factors that have stalled probiotic development previously[25]. Selection of these probiotics based on their niche-exclusion capabilities, as demonstrated here, also has the potential to enable development of probiotics with better safety profiles. While probiotics with the ability to produce inhibitory small molecules can be identified easily, pathogens can rapidly evolve to evade this form of antagonism. In comparison, probiotics which occupy a niche may leave a pathogen with fewer strategies to evolve resistance allowing long term utility in the clinical and more predictable effects on health.

Another great challenge for clinical development of lower airway probiotics is potency. In order to allow for adequate oxygen exchange in the lungs, alveoli need to remain unobstructed and, thus, colonization of the lung with a large dose of bacteria may result in undesirable outcomes. Therefore, probiotics which require extremely low doses to achieve a protective effect are desirable. Our methodology shows potential for repurposing of organisms that are typically poor performers for use in highly potent multi-organism formulations.

In this work, we found that one way that multi-organism probiotics defend against a pathogen is through consumption of various glycolytic substrates. In particular, lactate consumption appears to be important for efficacy. Several studies have found that there is increased lactate in the lung due to inflammatory exacerbations, which could feed pathogen growth[26–28]. Theoretically, if probiotics that preferentially consume lactate can be designed, they may be useful in combating infections in those with inflammatory lung conditions such as cystic fibrosis, idiopathic pulmonary fibrosis, and chronic obstructive pulmonary disease[27–29].

Broadly, we propose that lower airway probiotics may have functionality by stopping the positive feedback loop of infection. In this model, pathogen infiltration into the lung and growth results in inflammation and cellular injury, causing a leak of nutrient-rich fluids into the alveolar compartment, which further promotes pathogen growth (Figure 6 (left))[15]. Lower airway probiotics might stop this feedback loop by depleting nutrient abundance in the local lung environment, thereby limiting pathogen growth (Figure 6 (right))[15]. For clinical development, understanding resource competition as a mode of protection is useful, as probiotics can be forward-designed to work optimally within these environments in order to maximize potency and efficacy.

The native respiratory tract microbiome, and its interactions with host cells and incoming pathogens, is poorly understood, making development of airway probiotics a challenge. As our knowledge grows, health-promoting functionalities could be introduced into the lower respiratory tract, through supplementation with microbiome constituents in unaltered state (as demonstrated here) or with engineered properties, such as novel metabolisms. For utility in the clinic, extensive testing will be needed to determine the safety and reliability of airway probiotics as alternatives or additions to antibiotic therapies. Work is currently underway to understand the generalizability of the findings here to models of other respiratory diseases.

Methods

Isolation and Culture of Bacteria

A *Burkholderia thailandensis* E264 strain that constitutively expresses GFP was provided by Daniel J. Hassett (University of Cincinnati College of Medicine; Cincinnati, OH)[30]. The candidate probiotic (CP) isolates were recovered from the lower respiratory tracts of healthy mice using a culturomics approach[31]. All animal work was conducted in accordance with protocols approved by the Lawrence Livermore National Laboratory (LLNL) Institutional Animal Care and Use Committee (IACUC, protocol 304) and Institutional Biosafety Committee (IBC, protocol 2021-010). LLNL is accredited by the

Association for Assessment and Accreditation of Laboratory Animal Care (AAALAC) International, and is Public Health Service-Assured (PHS assurance A3184-01). Briefly, airway (trachea and lung) tissues were collected from 24 mice (C57Bl/6j, 10-20 weeks), homogenized in 500 uL of phosphate-buffered saline (PBS), and used to inoculate five different solid growth media [tryptic soy (TS); TS + 5% sheep's blood; M9 minimal salts + 0.2% glucose; brain-heart infusion (BHI); and lysogeny broth (LB) (Teknova; Hollister, CA)] as well as three different BACTEC blood bottles [Plus Aerobic/F; Plus Anaerobic/F; and Lytic/10 Anaerobic/F (Becton Dickinson; Franklin Lakes, NJ)]. The inoculated solid growth media were incubated at 37C for seven days. The inoculated blood bottles were incubated with shaking (250 rpm) for 1-5 days, and 100 uL aliquots were periodically withdrawn for use in inoculating the five different solid growth media, which were then incubated at 37C for seven days. All colonies detected on the solid growth media were individually transferred to LB agar and, after further incubation at 37C for 1-3 days, streaked to single colonies on fresh LB agar. A representative single colony from each Petri plate was used to inoculate LB liquid and solid media, and these cultures incubated at 37C for 1-3 days for use in preparing frozen glycerol stocks as well as extraction of genomic DNA for sequencing.

Genome Sequencing and Analysis

Extraction of high molecular weight DNA from overnight cultures of CPs was accomplished using the Nanobind CBB kit (PacBio catalog no.102-301-900). Barcoded sequencing libraries were prepared using the SMRTbell prep kit 3.0 (PacBio catalog no.102-141-700) with SMRTbell barcoded adapter 3.0 (PacBio catalog no.102-009-200) and using the Covaris g-TUBE shearing method to generate DNA fragments of 7-12 kb in length. Quantification of DNA concentrations was accomplished using the Qubit fluorometer method. The barcoded libraries were sequenced using a PacBio Sequel IIe system with HiFi workflows; one SMRT Cell 8M was used for run times of 15 hrs.

Genomic DNA extracted from each CP isolate was sequenced using an Illumina NextSeq 550 instrument (150SE reads). Raw sequencing reads were assembled using canu v2.2 using standard options[32]. Resultant contigs were manually inspected and BLAST was used to determine and remove duplicate assembled contigs. Phylogenetic placement in the GTDB release 202 system used the ANI-based script speciate.pl[33,34]. Phylogenomic analysis (Figure 1A) was performed using Species Tree Builder in KBase[35]. Genome assemblies were submitted to NCBI; assembly IDs are forthcoming.

Lung Simulating Medium (LSM) preparation

LSM was made according to Palmer (2006)[17]. Adjustments were made to the original formulation to increase sodium and chloride concentrations to more closely match those in healthy lungs. As a result, LSM contains 92mM NaCl instead of 66.6mM in SCFM[36]. Glucose concentration was also increased to 5.5mM.

Competition Assays

3ml overnight cultures were prepared at 37C and 278rpm of individual CPs and *Bt* in LSM from a stab of glycerol stock. After incubation for 24 hours, cultures were diluted again in LSM at a 1:50 and grown until late log phase. All cultures were spun down and resuspended in fresh LSM. CPs were diluted according to the ratios being tested where a 1:1 ratio represented a cell suspension of 3.33E4 CFU/mL of CP, 0.1 ratio represented 3.33E3 CFU/mL etc. After dilution, 3.33E4 CFU/ml of *Bt* was added to each 15ml CP dilution tube and a *Bt*-only control. The 15ml volume was split into 5-3ml to make biological replicates. All samples were incubated at 37C overnight with shaking at 278rpm.

After 24 hours, samples were removed and diluted 1:100-1:100,000 in PBS and plated onto LB carbenicillin100 to select for colonies of *Bt*. Plates were incubated for ~48 hours at 37C or until colonies were visible. Quantification was done by counting colonies. Percent *Bt* growth was calculated by taking the CFU/ml of each replicate culture and dividing by the average of the CFU/ml in the *Bt*-only control and multiplying by 100. Dose-response analysis was performed using the ECAnything algorithm in Graphpad Prism 10.

Supernatant inhibition experiments

CPs and *Bt* were grown overnight in LSM as previously described. Cultures were diluted to 5E5 CFU/ml and each CP was combined with *Bt*, a *Bt*-only control was also grown. After ~72 hours of growth, cultures were centrifuged and supernatant was collected and sterile filtered with a 0.22uM filter. All supernatant samples were pH adjusted to 7.03. Twice concentrated LSM and supernatant were mixed 1:1 and exponential-phase *Bt* was added to each sample at 3.33E4 CFU/mL. Growth curves were performed using a Tecan Spark plate reader measuring OD600 for 30 hours with shaking at 240rpm and 37C.

CP8 sfp knockout

The CP8Δ*sfp* mutant was made by the double-crossover homologous recombination method described previously[37]. Briefly, homologous arms were amplified up and

downstream of the *sfp* region and cloned into the T2(2)-ori plasmid in addition to the oriT/traJ region using golden gate assembly. The resulting plasmid was conjugated into CP8 using an established method for conjugation in *Bacillus* [38]. The conjugation was plated onto LB supplemented with Kanamycin20 and Polymyxin5 to select for *Bacillus* colonies containing the plasmid. Colonies were outgrown in LB Kanamycin 20 broth and subsequently incubated at 45C on LB Kan20 agar overnight to facilitate the first crossover event. A single colony positive for the first crossover event was selected and subsequently passaged in LB broth 6 times. Replica plating was performed to check for loss of kanamycin resistance and PCR was used to screen for colonies where *sfp* was absent. Resulting fragments and 16S region were sequenced to confirm deletion and strain identity.

Overlay assays

Overnight cultures of *Bt* and CP8 were made in LSM as previously described. *Bt* was diluted to OD 0.5 and streaked onto LSM agar using a sterile cotton swab. Plates were briefly allowed to dry and 2ul spots of CP8 overnight culture were added. Plates were incubated overnight and checked for the appearance of a zone of inhibition after 48 hours.

Carbon source screening

Overnight cultures of CPs and *Bt* in LSM were made as previously described. Cultures were centrifuged and washed twice with 2x LSM with carbon sources removed. Cultures were diluted to an OD of 0.04 added to a 384-well plate containing all carbon sources from LSM medium at a concentration of 10mM. Initial OD600 readings were taken using a plate reader prior to incubation. Plates were subsequently incubated at 30C for 3 days at 800rpm and a plate reader was used to take their final OD600 reading. Each CP or *Bt* was considered able to utilize a given carbon source if the final OD600 reading was greater than the blank plus 2 standard deviations.

Exometabolomics

Overnight cultures of CP7, CP8, CP19 and *Bt* were made as previously described. Cultures were backdiluted 1:50 and grown to late log phase. Cultures were made in LSM combining *Bt* at 3.33E4 CFU/ml with the relevant CP at the IC90 for the individual CP. Cultures were incubated at 37C with shaking at 278rpm and samples were collected at 24 and 36 hours. For collection, samples were centrifuged at 3000rcf for 10 minutes. Supernatant was removed and syringe filtered to remove residual cellular material. Samples were analyzed via GC-TOF by the West Coast Metabolomics Center.

Data was SERRF normalized to remove batch effect then normalized to the amount injected. Metabolite concentrations were normalized to a media-only control. For analysis, concentrations of each metabolite were converted to metabolite-contributed electrons using the oxidation-reduction half reaction for each metabolite analyzed. For carbon subset analysis, total electrons from lactate, proline, and aspartic acid in the co-culture supernatant at 24 hours were added. Electron concentrations below 0 indicate that a given metabolite is more abundant in co-culture than the media control.

Pairwise Combination Competition Assays

Pairwise combination competition assays were performed as described in “Combination Competition Assays” with the following adjustments. After resuspension in fresh media, the two CPs of interest were mixed at a 1:1 ratio at the desired CFU/ml (eg. for a 1:1 ratio with *Bt*, a 3.33E4 CFU/ml CP mixture was made). Subsequent dilutions were made and carried out as previously described.

Bliss Independence Model

The Bliss independence model was used to calculate the expected combined effect of two CPs on *Bt* growth. The expected effect is calculated as follows:

$$Expected\ Effect = E_A + E_B(100 - E_A)$$

Where E_A and E_B are the percent inhibition of *Bt* when co-cultured with each CP alone. When the observed effect is greater than the expected effect, a combination is determined to have synergy. For combinations in which one or both CPs do not show inhibition in pairwise co-culture with *Bt*, Bliss independence cannot be calculated.

Animal Model

These studies were carried out in strict accordance with the recommendations in the *Guide for the Care and Use of Laboratory Animals* and the National Institute of Health. All efforts were made to minimize suffering of animals. All animals were housed in ABSL2 conditions in an AAALAC-accredited and PHS-assured facility, and the protocol was approved by the Lawrence Livermo National Laboratory Institutional Animal Care and Use Committee (IACUC), which includes ethics in evaluation of protocols. Barrier-housed, specific pathogen-free C57Bl/6j mice and acclimated prior to experiments. CP, *Burkholderia thailandensis*, and animal use was also approved by the Institutional Biosafety Committee (IBC).

Colonization Studies

Each CP was grown in monoculture in LB at 37C with shaking (250 rpm) for 16 h, recovered through centrifugation, resuspended in PBS, and diluted to an OD600 corresponding to 3.3E7 CFU/mL (based on prior determination of OD600-to-CFU plating efficiency measurements). 30 ul of this dosing material (corresponding to 10^6 CFU) were administered to the airway (via OPA) of a C57Bl/6j mouse. After 7 days, the trachea and lungs were collected and homogenized in PBS; dilutions (in PBS) were plated on LB agar; and, after 1-5 days at 37C, the CFU enumerated in order to assess CP load in the airway

Survival Studies

CP dosing material was generated and administered to mice as described above. After 3, 5 or 7 days, 6-week old mice were similarly administered 3E4 - 5E5 CFU of *Bt* via OPA. Weight, morbidity, and mortality were monitored for 10 days following *Bt* challenge; mice displaying >=20% loss of body weight were euthanized.

Statistical analyses

Ordinary one-way ANOVA with Tukey's multiple comparisons test, ROC curve analyses, Mantel-Cox survival analyses and all plotting was completed in Graphpad Prism 10.

Author Contributions

K.E.H., S.S.B. and A.P.A. conceived the study. N.M.C, A.M.P. and S.S.B. performed isolation work. C.M.M., K.P.W. and A.S. sequenced and analyzed genomes. K.E.H. carried out in vitro experiments with contributions from H.K.C., and analyzed the data. N.M.C, A.M.P. and S.S.B. performed *in vivo* work. K.E.H. wrote the paper with contributions from S.S.B. and A.P.A and feedback from all authors.

Acknowledgements

We thank K. Sander (UCB) and K. Vyas (CMS) for helpful discussion; D. Sivanandan (UCB) for assistance with experiments. We thank the West Coast Metabolomics Center for exometabolomics services. Sandia National Laboratories is a multimission laboratory managed and operated by National Technology & Engineering Solutions of Sandia, LLC, a wholly owned subsidiary of Honeywell International Inc., for the U.S. Department of Energy's National Nuclear Security Administration under contract DE-NA0003525. This work was supported by funding from the U.S. Department of Energy, Laboratory

Directed Research and Development Award, through Sandia National Laboratories (award number 218309). This paper describes objective technical results and analysis; any subjective views or opinions that might be expressed in the paper do not necessarily represent the views of the U.S. Department of Energy or the United States Government. This work was performed under the auspices of the U.S. Department of Energy by Lawrence Livermore National Laboratory under contract DE-AC52-07NA27344. K.E.H. thanks the National Defense Science and Engineering Graduate Fellowship Program for support.

References:

1. Costello, E. K. *et al.* Bacterial community variation in human body habitats across space and time. *Science* **326**, 1694–1697 (2009).
2. Santacroce, L. *et al.* The Human Respiratory System and its Microbiome at a Glimpse. *Biology* **9**, (2020).
3. Man, W. H., de Steenhuijsen Piters, W. A. A. & Bogaert, D. The microbiota of the respiratory tract: gatekeeper to respiratory health. *Nat. Rev. Microbiol.* **15**, 259–270 (2017).
4. Das, S. *et al.* A prevalent and culturable microbiota links ecological balance to clinical stability of the human lung after transplantation. *Nat. Commun.* **12**, 2126 (2021).
5. Bäumler, A. J. & Sperandio, V. Interactions between the microbiota and pathogenic bacteria in the gut. *Nature* **535**, 85–93 (2016).
6. Kamada, N., Chen, G. Y., Inohara, N. & Núñez, G. Control of pathogens and pathobionts by the gut microbiota. *Nat. Immunol.* **14**, 685–690 (2013).
7. Fangous, M. S. *et al.* Lactobacilli intra-tracheal administration protects from Pseudomonas aeruginosa pulmonary infection in mice - a proof of concept. *Benef. Microbes* **10**, 893–900 (2019).
8. Soner Yildiz, João P Pereira Bonifacio Lopes, Matthieu Bergé, Víctor González-Ruiz, Damian Baud, Joachim Kloehn, Inês Boal-Carvalho, Olivier P Schaeren, Michael Schotsaert, Lucy J Hathaway, Serge Rudaz, Patrick H Viollier, Siegfried Hapfelmeier, Patrice Francois, Mirco Schmolke. Respiratory tissue-associated commensal bacteria offer therapeutic potential against pneumococcal colonization. *eLife* (2020).
9. Fauroux, B. *et al.* Burkholderia cepacia is associated with pulmonary hypertension and increased mortality among cystic fibrosis patients. *J. Clin. Microbiol.* **42**, 5537–5541 (2004).
10. Coenye, T., Vandamme, P., Govan, J. R. & LiPuma, J. J. Taxonomy and identification of the Burkholderia cepacia complex. *J. Clin. Microbiol.* **39**, 3427–3436 (2001).
11. Yu, Y. *et al.* Genomic patterns of pathogen evolution revealed by comparison of

Burkholderia pseudomallei, the causative agent of melioidosis, to avirulent Burkholderia thailandensis. *BMC Microbiol.* **6**, 46 (2006).

12. Brett, P. J., DeShazer, D. & Woods, D. E. Burkholderia thailandensis sp. nov., a Burkholderia pseudomallei-like species. *Int. J. Syst. Bacteriol.* **48 Pt 1**, 317–320 (1998).
13. Kim, H. S. *et al.* Bacterial genome adaptation to niches: divergence of the potential virulence genes in three Burkholderia species of different survival strategies. *BMC Genomics* **6**, 174 (2005).
14. Günther, A. *et al.* Surfactant alterations in severe pneumonia, acute respiratory distress syndrome, and cardiogenic lung edema. *Am. J. Respir. Crit. Care Med.* **153**, 176–184 (1996).
15. Dickson, R. P., Erb-Downward, J. R. & Huffnagle, G. B. Towards an ecology of the lung: new conceptual models of pulmonary microbiology and pneumonia pathogenesis. *Lancet Respir Med* **2**, 238–246 (2014).
16. Dickson, R. P. & Huffnagle, G. B. The Lung Microbiome: New Principles for Respiratory Bacteriology in Health and Disease. *PLoS Pathog.* **11**, e1004923 (2015).
17. Palmer, K. L., Aye, L. M. & Whiteley, M. Nutritional cues control Pseudomonas aeruginosa multicellular behavior in cystic fibrosis sputum. *J. Bacteriol.* **189**, 8079–8087 (2007).
18. Lloyd, D. P. & Allen, R. J. Competition for space during bacterial colonization of a surface. *J. R. Soc. Interface* **12**, 0608 (2015).
19. van Gestel, J., Weissing, F. J., Kuipers, O. P. & Kovács, A. T. Density of founder cells affects spatial pattern formation and cooperation in Bacillus subtilis biofilms. *ISME J.* **8**, 2069–2079 (2014).
20. Aiosa, N. *et al.* Whole-Cell MALDI-ToF MS Coupled with Untargeted Metabolomics Facilitates Investigations of Microbial Chemical Interactions. *Chembiochem* **24**, e202200802 (2023).
21. Vecchio-Pagan, B., Bewick, S., Mainali, K., Karig, D. K. & Fagan, W. F. A Stoichioproteomic

Analysis of Samples from the Human Microbiome Project. *Front. Microbiol.* **8**, 1119 (2017).

22. Rohmer, L., Hocquet, D. & Miller, S. I. Are pathogenic bacteria just looking for food? Metabolism and microbial pathogenesis. *Trends Microbiol.* **19**, 341–348 (2011).
23. Foucquier, J. & Guedj, M. Analysis of drug combinations: current methodological landscape. *Pharmacol Res Perspect* **3**, e00149 (2015).
24. Yagi, K., Huffnagle, G. B., Lukacs, N. W. & Asai, N. The Lung Microbiome during Health and Disease. *Int. J. Mol. Sci.* **22**, (2021).
25. de Melo Pereira, G. V., de Oliveira Coelho, B., Magalhães Júnior, A. I., Thomaz-Soccol, V. & Soccol, C. R. How to select a probiotic? A review and update of methods and criteria. *Biotechnol. Adv.* **36**, 2060–2076 (2018).
26. De Backer, D., Creteur, J., Zhang, H., Norrenberg, M. & Vincent, J. L. Lactate production by the lungs in acute lung injury. *Am. J. Respir. Crit. Care Med.* **156**, 1099–1104 (1997).
27. Bensel, T. *et al.* Lactate in cystic fibrosis sputum. *J. Cyst. Fibros.* **10**, 37–44 (2011).
28. Kottmann, R. M. *et al.* Lactic acid is elevated in idiopathic pulmonary fibrosis and induces myofibroblast differentiation via pH-dependent activation of transforming growth factor-β. *Am. J. Respir. Crit. Care Med.* **186**, 740–751 (2012).
29. Lozo Vukovac, E. *et al.* Bronchoalveolar pH and inflammatory biomarkers in patients with acute exacerbation of chronic obstructive pulmonary disease. *J. Int. Med. Res.* **47**, 791–802 (2019).
30. Su, S. *et al.* Construction and characterization of stable, constitutively expressed, chromosomal green and red fluorescent transcriptional fusions in the select agents, Bacillus anthracis, Yersinia pestis, Burkholderia mallei, and Burkholderia pseudomallei. *Microbiologyopen* **3**, 610–629 (2014).
31. Lagier, J.-C. *et al.* Microbial culturomics: paradigm shift in the human gut microbiome study. *Clin. Microbiol. Infect.* **18**, 1185–1193 (2012).
32. Koren, S. *et al.* Canu: scalable and accurate long-read assembly via adaptive k-mer

weighting and repeat separation. *Genome Res.* **27**, 722–736 (2017).

33. Parks, D. H. *et al.* GTDB: an ongoing census of bacterial and archaeal diversity through a phylogenetically consistent, rank normalized and complete genome-based taxonomy. *Nucleic Acids Res.* **50**, D785–D794 (2022).
34. Mageeney, C. M., Trubl, G. & Williams, K. P. Improved Mobilome Delineation in Fragmented Genomes. *Front Bioinform* **2**, 866850 (2022).
35. Arkin, A. P. *et al.* KBase: The United States Department of Energy Systems Biology Knowledgebase. *Nat. Biotechnol.* **36**, 566–569 (2018).
36. Jayaraman, S., Joo, N. S., Reitz, B., Wine, J. J. & Verkman, A. S. Submucosal gland secretions in airways from cystic fibrosis patients have normal [Na^+] and pH but elevated viscosity. *Proceedings of the National Academy of Sciences* **98**, 8119–8123 (2001).
37. Qi, G. *et al.* Deletion of meso-2,3-butanediol dehydrogenase gene budC for enhanced D-2,3-butanediol production in Bacillus licheniformis. *Biotechnol. Biofuels* **7**, 16 (2014).
38. Heinze, S. *et al.* Transmating: conjugative transfer of a new broad host range expression vector to various Bacillus species using a single protocol. *BMC Microbiol.* **18**, 56 (2018).

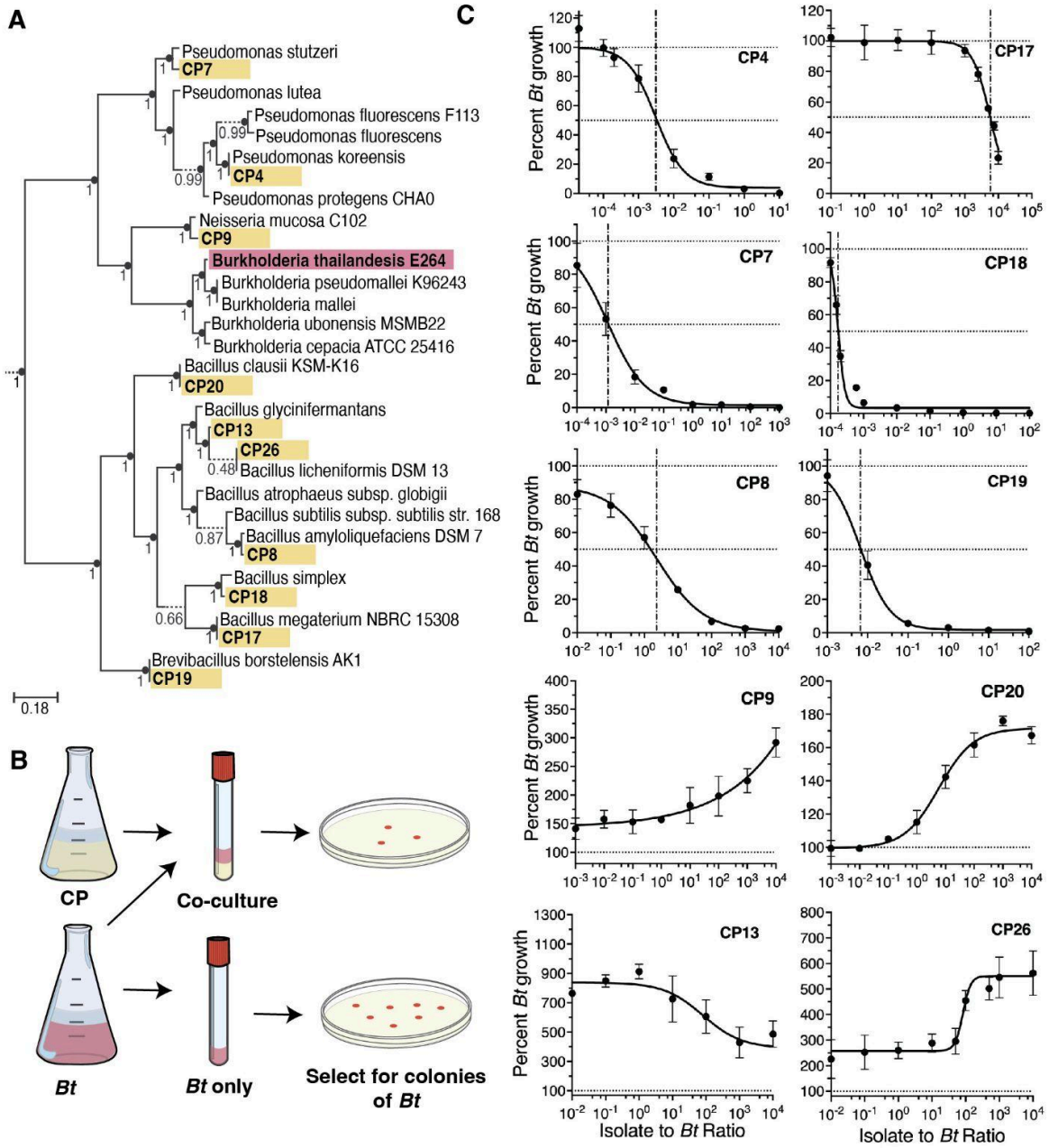

Figure 1 Characterization of CP activity against *B. thailandensis in vitro.* **a**, Phylogenomic tree of CPs (yellow) and model pathogen, *B. thailandensis* (red), interspersed amongst publicly available genomes (no color). **b**, Schematic of competition assay used to test *in vitro* inhibitory capabilities of CPs. Percent growth of *Bt* is calculated as the CFU in co-culture/CFU in *Bt* only culture multiplied by 100. Co-culture inhibition was tested and calculated for multiple starting densities of CP (see Figure 1C x-axis). **c**, Dose-response curves for CPs against *B. thailandensis.* Relative IC50 is denoted with a vertical dashed-dotted line and horizontal 100% and 50% growth marked with dotted lines.

Table 1 | **Summary of CP activity**

CP	Species	Relative IC50	95% Confidence Interval (CI)	Bt growth at a 1:1 ratio (%)	Niche Index
CP7	*Pseudomonas stutzeri*	0.001172	0.0006442 - 0.003346	1.89	0.875
CP4	*Pseudomonas fluorescens*	0.003086	0.001791 - 0.005331	3.20	0.869
CP19	*Brevibacillus borstelensis*	0.006604	0.0064842 - 0.01141	3.05	0.775
CP17	*Bacillus megaterium*	5738	3598 - ND**	98.99	0.704
CP18	*Brevibacterium frigoritolerans*	0.0001693	0.0001633 - 0.0001850	0.53	0.591
CP20	*Bacillus clausii*	Non-inhibitory*	N/A	115.19	0.457
CP26	*Bacillus licheniformis*	Non-inhibitory*	N/A	259.99	0.433
CP13	*Bacillus licheniformis*	Non-inhibitory*	N/A	913.04	0.421
CP9	*Neisseria lactamica*	Non-inhibitory*	N/A	157.143	0.357
CP8	*Bacillus velezensis*	2.316	0.8280 - 5.073	56.97	0.351

Less niche overlap with *Bt*

***Non-inhibitory CPs do not have relative IC50 values associated with them**

****value could not be determined**

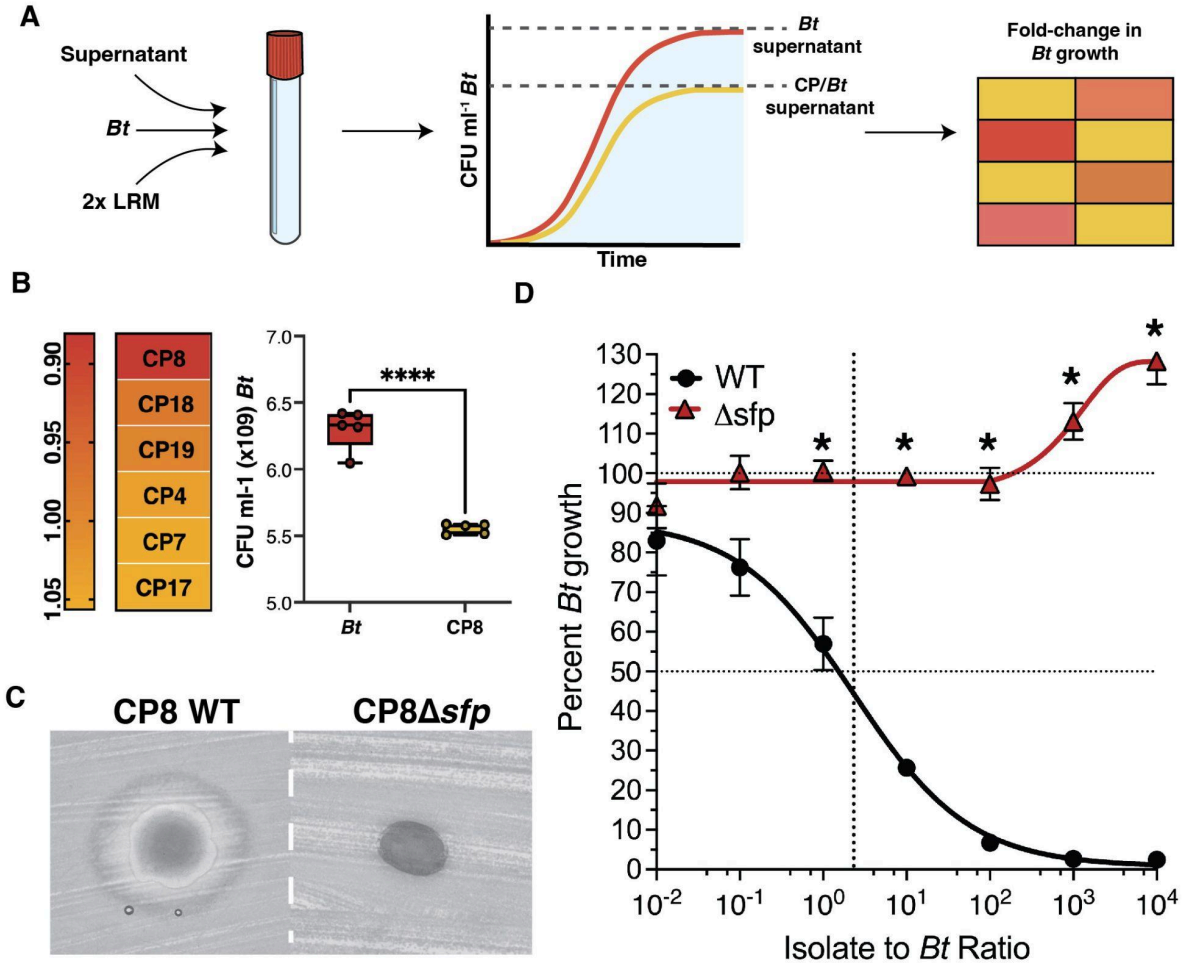

Figure 2 Specialized metabolites play a role in antagonistic activities of CPs. a, Schematic representation of supernatant workflow. **b**, (left) Heatmap of fold-change in max CFU from supernatant of each inhibitory CP relative to *B. thailandensis* grown in supernatant from itself. **c**, Overlay assays of wildtype (CP8 WT) CP8 and *sfp* mutant (CP8Δ*sfp*).**d,** Dose-response curve of wildtype CP8 and *sfp* mutant against *B. thailandensis*

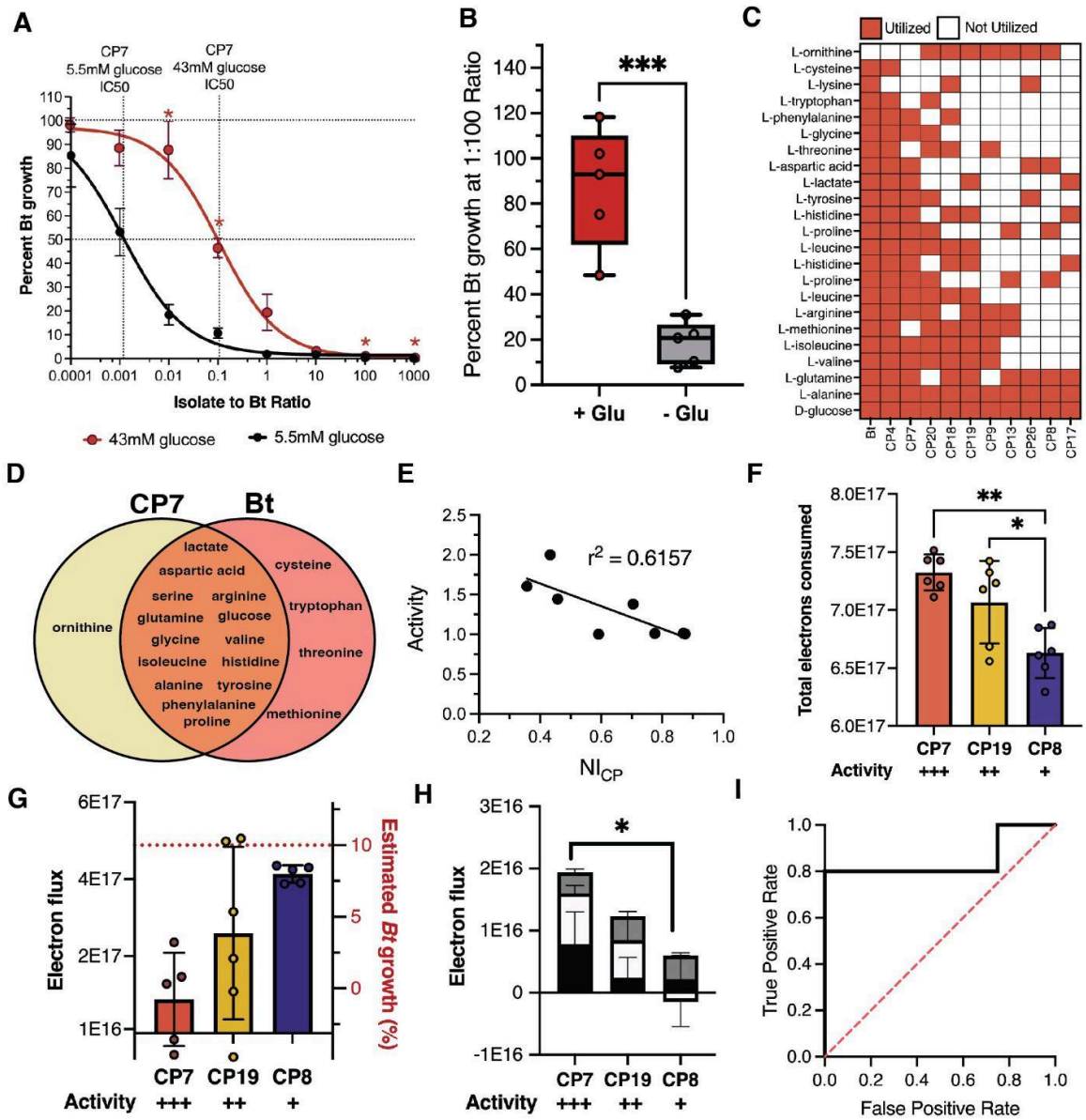

Figure 3 Niche overlap is the primary mode of inhibition for CPs. a, Dose-response curve for CP7 grown in unsupplmented LRM (black) or with additional glucose (red) **b,** Activity of CP7 against *Bt* at a 1:100 with or without glucose supplementation **c**, Carbon utilization heatmap for all CPs in the panel and *Bt* **d,** Venn diagram of carbon sources utilized by CP7 and *Bt* **e,** Correlation between average normalized growth of *Bt* at a 1:1 ratio and Niche Index **f,** Total carbon consumed by 3 isolates grown in combination with *Bt* at 36 hours **g,** Total electron flux at 24 hours, red dashed line indicates the estimated abundane of *Bt* in each co-culture **h,** Electron flux of lacate (black), proline (white) and aspartic acid (gray) at 24hrs in differnet isolate co-culture conditions **i,** Receiver operator characteristic curve showing the ability of growth on lactate to distinguish inhibitory CPs from non-inhibitory CPs. An AUROC of 1 indicates perfect distinction while the dashed red line represents an AUROC of 0.5 indicating no distinction between inhibitors and non-inhibitors.

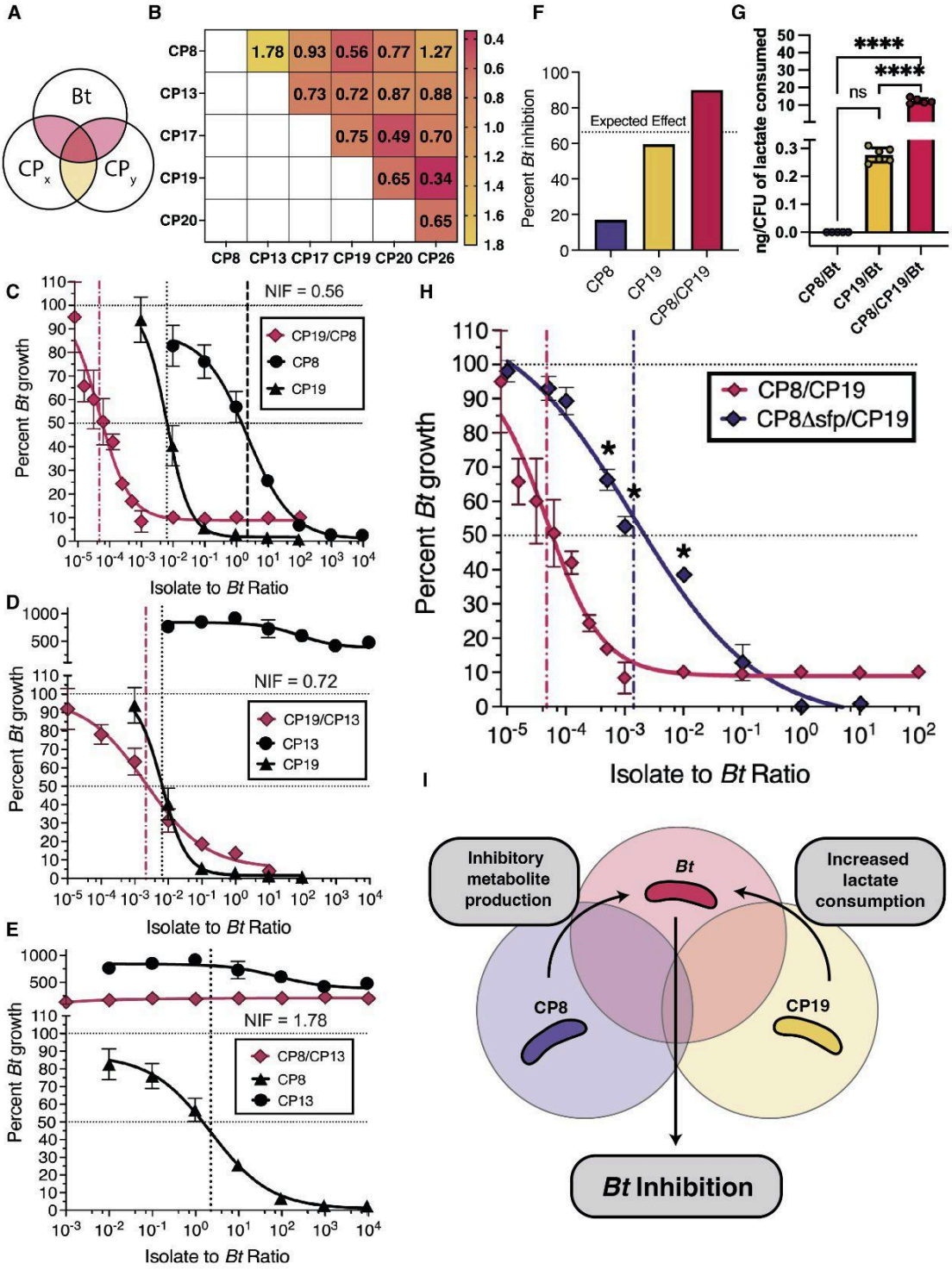

Figure 4 Niche overlap aids in identification of effacious combinations. a,Diagramatic representation of the Niche Index Fraction (NIF) calculation. Yellow represents the fraction numerator and red, the denominator. **b,** Heatmap of NIFs for each colonizing CP. **c,** Dose-response curve for a combination of CP8/CP19 **d,** Dose-response curve for a combination of CP19/CP13 **e,** Dose-response curve for a combination of CP13/CP8 **f,** Bliss independence calculation for the CP8/CP19 combination, dashed line indicates the expected effect for CP19 and CP8 used in combination. Calculated values above the line represent synergy and below the line, antagonism **g,** Lactate consumed determined via GC-TOF for 3 conditions normalized to CFU of each CP inoculated **h,** Dose-response curve for a combination of CP8/CP19 and CP8Δ*sfp*/CP19 **i,** Proposed mechanism for CP8/CP19 combination inhibition. CP8 produces a specialized metabolite which inhibits growth of the pathogen. Increased lactate consumption by CP19 in the presence of CP8 also creates nutrient competition with *Bt*. Overall, little niche overlap between the CPs and high overlap with *Bt* allows further inhibition of the pathogen with minimal inter-CP competition.

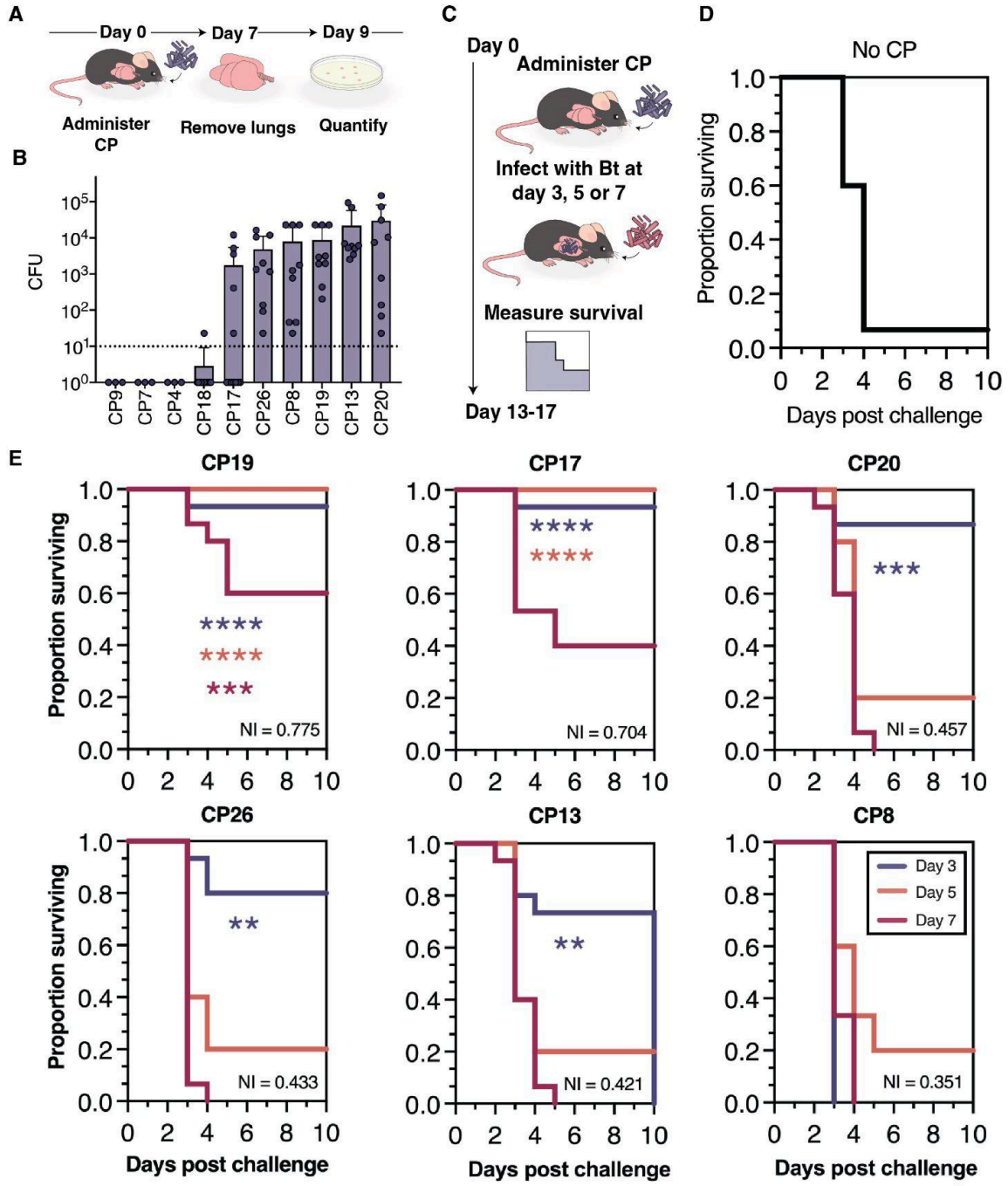

Figure 5 CPs enhance survival *in vivo*. a, Schematic of engraftment testing for CPs. 10^6 CFU of each CP is administered via OPA and lungs are removed for CFU quantification after 7 days **b,** Colonization results from homogenized lung tissue from 7 days after CP administration. The dotted line represents the minimum CFU at which a CP is considered able to colonize **c,** Schematic of method for survival testing. Mice were administered 10^6 CFU of each CP and then challenged with pathogen at days 3, 5 or 7. Survival was measured for 10 days following challenge **d,** Survival data from mice administrered vehicle control **e,** Survival data from mice administered CPs 3 days (blue), 5 days (orange) or 7 days (red) prior to pathogen challenge. Niche Index values are listed in the lower right corner for each CP.

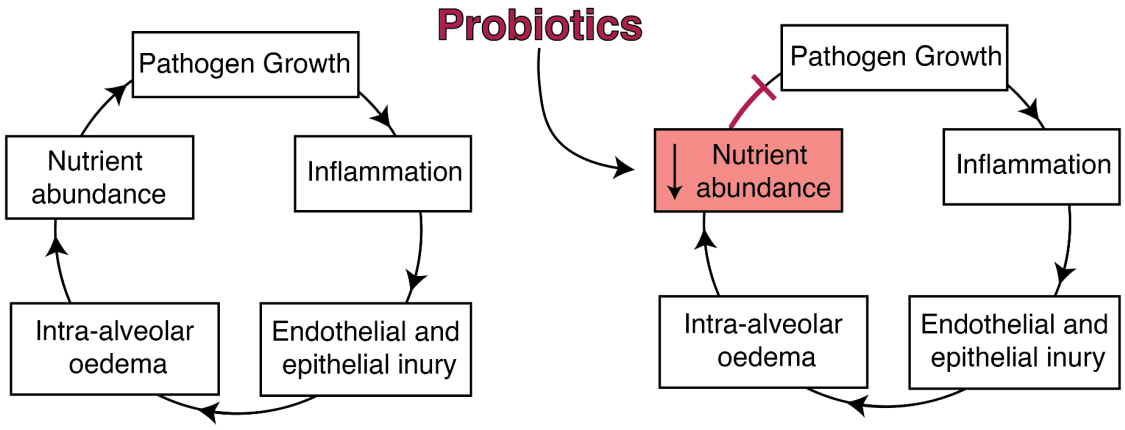

Figure 6 Proposed mechanism of CP protection. During lung infection (left) bacterial growth elicits inflammation from the host with concurrent endothelial and epithelial injury. Intra-alveolar oedema introduces additional nutrients from the blood into the lung alveoli and lumen allowing for increased bacterial growth of the pathogen. This positive feedback loop allows uncontrolled growth of the pathogen ultimately facilitating instantation of infection. We proposes that probiotics delivered directly to the lung may limit infection by reducing nutrient abundance after oedema (right). Limited nutrient abudance inhibits bacterial pathogen growth and rapidly ends the infection-promoting feedback loop.